J. Astrophys. Astr. (2023) 44:29
https://doi.org/10.1007/s12036-023-09929-9

Difference analysis of temporal evolution and shape of hemispheric sunspot cycles

JUAN ZHAO* and YANG CHEN

Department of Astronomy, Beijing Normal University, Beijing 100875, People's Republic of China.
Corresponding author. E-mail: zj@bnu.edu.cn

MS received 28 March 2022; accepted 1 December 2022

Abstract. This paper focuses on the temporal evolution and shape of northern and southern hemispheric sunspot number. The comparisons, whether from time-varying spectral analysis or global power spectrum before and after filtering, imply the similarity and difference in the characteristics of periods between the northern and southern hemispheres. We have decomposed monthly hemispheric standardized sunspot of cycles 19–24 using principal component (PC) analysis and reconstructed based on the three principal components. These exhibit different characteristics of variation. And the main determinant of variation in various cycles is the second and third PC, whatever the hemisphere is. The comparisons we have outlined imply the hemispheric asymmetry. The difference analysis of the temporal evolution, shape of hemispheric sunspot cycles, and asymmetry is of great importance in understanding the global cycle variation and its evolution to fully understand the physical mechanism of the solar periodic variation and hemispheric asymmetry.

Keywords. Sunspot cycle—hemisphere—spectrum—principal component analysis.

1. Introduction

Sunspots are important surface manifestations of solar activity. Each sunspot has strong magnetic field and often appears in pairs. The polarity of the leading and trailing parts of a sunspot is opposite in two hemispheres. However, there is a change in polarity order in the northern and southern hemispheres in the next cycle. The distribution of magnetic field polarity with solar cycle variation follows Hale polarity law, should be about 22 years, known as the solar magnetic cycle (Hale & Nicholson 1925).

In recent years, much attention has been paid to the hemispheric sunspot number followed with solar activity and its variation and reveal significant asymmetry in the northern and southern hemispheres (Jennings & Weiss 1991; Hathaway 2015; Takalo & Mursula 2020; Prithvi 2021). Waldmeir (1960) suggested that the polar shift in the south pole region and earlier in the north pole region may be related to the fact that sunspot in the southern hemisphere reach the maximum before those in the northern hemisphere.

From analyzing the solar activity in the decade 1959–1969, Waldmeier (1971) pointed out the most outstanding feature is the extraordinarily strong asymmetry on the two hemispheres. On the northern hemisphere, spots, faculae and prominences were more numerous and the white light corona was brighter than that on the southern hemisphere. The solar polar field reversal times are also not the same. For example, the strongly asymmetric solar cycle 19, when the southern hemisphere was most active before sunspot maximum and the south pole duly reversed first, followed by the northern hemisphere more than a year later, when that hemisphere became the most active (Svalgaard & Kamide 2013).

It has been shown for various solar indices related to surface magnetism that there exist significant asymmetries. Tobias (1997) pointed the magnetic field is significantly modulated, whilst staying largely dipolar. The field is no longer symmetric and magnetic activity is confined to one hemisphere when the field is weak. North–south asymmetries have also been identified in Joy's law. The mean tilt angle

Published online: 03 April 2023

observed in solar cycle C16–C21 was significantly different in the northern and southern hemispheres (Mcclintock & Norton 2013). Schüssler & Cameron (2018) analyzed the origin of the hemispheric asymmetry of solar activity and suggested that it can be naturally explained by the superposition of an excited dipolar mode (toroidal field antisymmetric with respect to the equator) with a magnetic period of about 22 years and a linearly damped, but randomly excited quadrupolar mode (toroidal field symmetric with respect to the equator) with a period between 13 and 15 years.

The characteristics of hemispheric sunspot cycle have always been a very important research field. For example, it should be necessary to fully understand the physical mechanism of the solar periodic variation and hemispheric asymmetry and help us to improve the solar activity prediction more accurately. Further, studying the long-term evolution and change patterns of the solar cycle in both hemispheres is a crucial step toward revealing the solar dynamo process behind this evolution (Sokoloff & Nesme 1994; Norton *et al.* 2014). And it is the fundamental and essential question of solar physics.

In this paper, we present a special way, using principal component analysis (PCA), to decompose the hemispheric SN series into components to focus on the temporal variation and the shape in the character and rules of hemispheric solar cycles.

2. Data

The monthly hemispheric relative sunspot number (SN) is based on data from the Uccle station (https://www.sidc.be/silso/) from July 1950 up to June 1994, and the new version data starting from January 1992 from the Royal Observatory of Belgium (http://www.sidc.be/silso/).

Owing to the short data series of the Royal Observatory of Belgium, to obtain more solar cycles, data from the Uccle station are selected at the same time. Overlap for the interval January 1992–June 1994 are shown in Figure 1(a, b). In order to be able to calibrate two series into a sequence, we standardized the series by having zero and divided by the standard deviation, respectively. The results are shown in Figure 1(c, d), and both have similar characteristics of change. Therefore, what we have done now is, to calibrate the two series to merge into a common homogeneous composite series through the standardized SN (SSN) from the Uccle station from July 1950 up to December

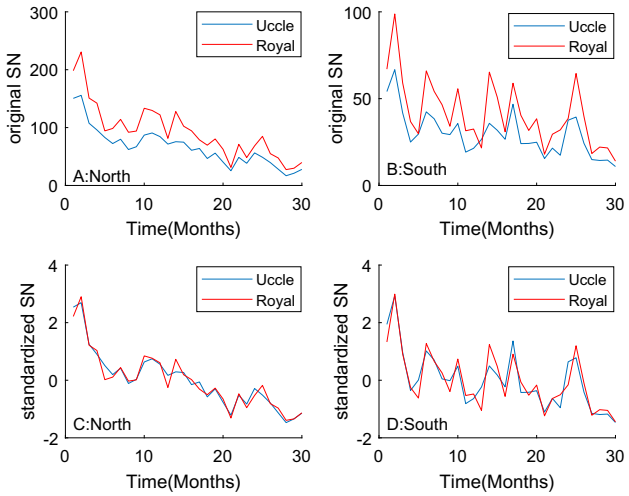

Figure 1. Comparison of the overlap from January 1992 to June 1994 between two series. Blue curves is from Uccle station and red curves is from Royal Observatory of Belgium. Top panel: Original monthly hemispheric SN. Bottom panel: Standardized monthly hemispheric SN series.

1991, and the standardized SN starting from January 1992 from the Royal Observatory of Belgium.

Evolution of the standardized hemispheric SN is plotted in Figure 2. Obviously, the monthly series still have bigger fluctuations, especially around the peak. Therefore, we applied 13-point moving average for the monthly series, with which the annual fluctuation will be effectively eliminated. We could clearly discern the differences in the phase, amplitude, peak shape and bimodal structure between the northern and southern hemispheric SN series.

As December 2019 was confirmed as starting point of the new solar cycle, solar activity has undergone six cycles since 1950. The smoothed series are divided into 12 completed cycles from C19 to C24 at the valley for the northern and southern hemispheres, respectively. The length of 12 cycles of two hemispheres are listed in Table 1.

We could note that the cumulative length of even–odd pairs of the northern hemisphere become approximately equal to that of the southern hemisphere, although the length of the individual cycles varies. In other words, with shorter length of cycle, the northern hemisphere precedes, with longer length of next cycle in the same hemisphere. Finally, the northern and southern hemispheres almost synchronized the pace to reach the starting point of next new cycle. For example, the length of northern C23 is shorter than its southern C23, but the length of northern C24 is longer than its southern C24.

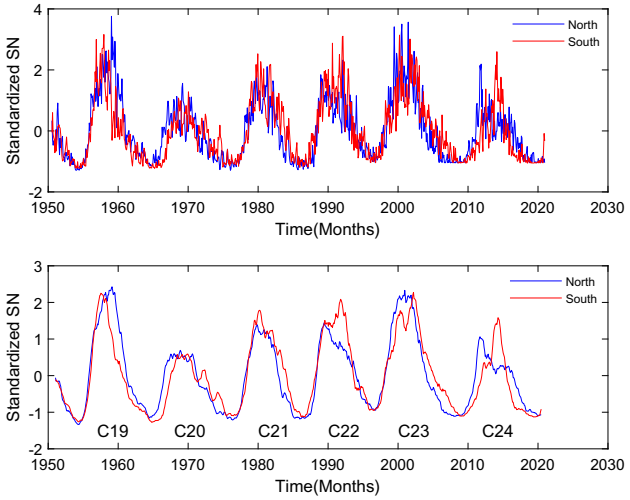

Figure 2. Monthly standardized values of hemispheric sunspot numbers from 1950 to 2020. Top panel: Blue (red) curves show the north (south) hemispheric standardized SN, respectively. Bottom panel: 13-month smoothed hemispheric standardized SN (north: blue, south: red), namely, cycles C19–C24.

Table 1. Sunspot cycle lengths (in months) and the cumulative length of adjacent cycles for cycles C19–C24.

Cycle	North	North (pairs)	South	South (pairs)
C19	122	–	127	–
C20	144	266	141	268
C21	116	–	118	–
C22	131	247	125	243
C23	135	–	152	–
C24	145	280	124	276

Notes: We list the cycle number, length of sunspot cycles for the northern and southern hemisphere, respectively, and the cumulative length of the two adjacent cycles.

According to the magnetic field transformation rule of the sunspots, a complete cycle takes about 22 years that is Hale-cycle thought to be caused by a dynamo mechanism operating in the solar interior. Therefore, the fact of even–odd pairs with the equal length is easily understood.

3. Spectrum analysis for hemispheric SSN

Wavelet analysis of hemispheric SSN display considerable frequency variation because the time and frequency character of the signal is combined very well through the wavelet spectrum. It easily shows the magnitude and intensity of periods with obvious time-varying characters (Figures 3 and 4). The top panels

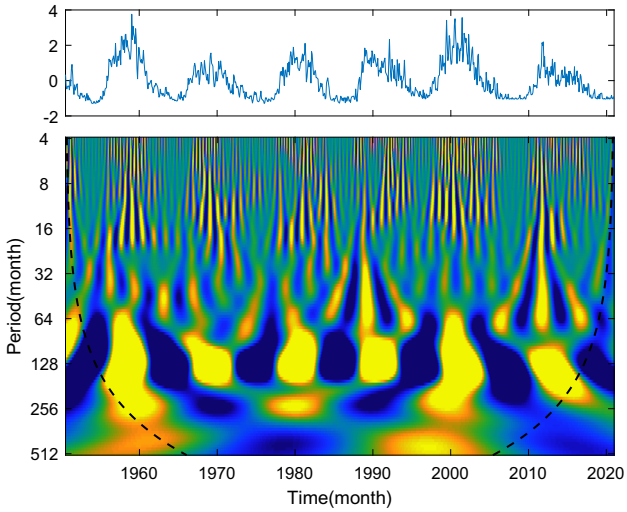

Figure 3. Top: Monthly standardized SN of the northern hemisphere for the time range 1950–2020. Bottom: Local wavelet power spectrum for the northern SSN (dashed line indicating the cone of influence is 90% confidence level).

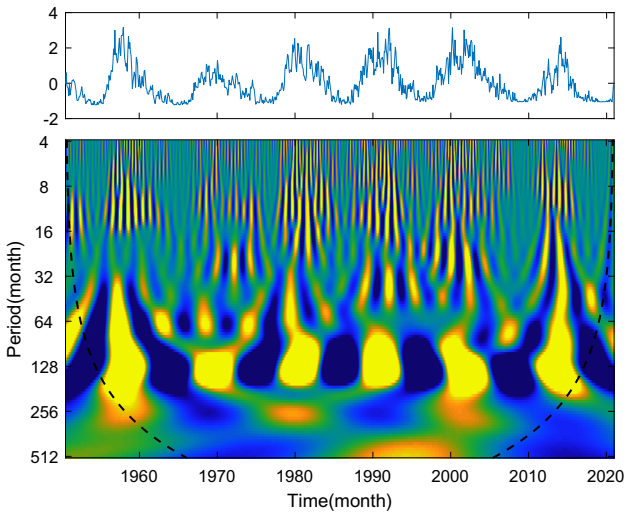

Figure 4. Top: Monthly standardized SN for the southern hemisphere for the time range 1950–2020. Bottom: Local wavelet power spectrum for the southern SSN (dashed line indicating the cone of influence is 90% confidence level).

are the standardized hemispheric SN series. The bottom panels show the wavelet power spectrum of northern and southern hemispheric SSN, respectively, and reveal that a high energy content corresponds to the Schwabe cycle ($\sim$11 years). In addition, hemispheric SSN has some evident short periods, between 2 and 7 years aside from the 11-year period. These short periods clearly exhibit the strong or weak features of solar activity, and are obviously regulated by the 11-year cycle. On the whole-time scale, short periods are very active when the solar activity is

strong. Conversely, the overall performance of the short periods is inactive when the activity is weak. Some periods do not last throughout the series. For example, the oscillations indicate that the activity about 40-month occurred obviously, but sometimes were relatively calm. The dashed lines in Figures 3 and 4 indicate the cone of influence (COI) that means the region below which suffers from edge effects due to the finite-length of signal.

As seen in Figures 3 and 4, the changes in the northern and southern hemispheres exist with a lot of consistency. However, the magnitude characteristics of different periods in different duration are quite inconsistent, especially in short periods.

Power spectra of the hemispheric SSN revealed obvious decadal-scale periods, such as about 11-year, and short periods about 2–7-years (Figure 5). This is consistent with the analysis aforementioned by wavelet analysis. We could note that the average length of Schwabe cycle varies for hemispheric monthly SSN for the time range of 1950–2020. The 120.5 months (frequency: 0.0083) in the northern hemisphere is shorter than the 140.8 months (frequency: 0.0071) in the southern hemisphere.

Because of the intense 11-year-period amplitude, it is hard to analyze the short periods. For a better understanding of the short periods from 20 to 80 months and its variation properties in hemispheric SSN, the filtering method helps us to separate the period components to eliminate or extract the component in digital signals. Therefore, it is applied to hemispheric SSN with the fast-Fourier transform (FFT) and inverse FFT (IFFT) to filter periods to remove the influence of the 11-year period. FFT and IFFT methods are usually used to realize the transformation between the time and frequency domain due to their good selectivity and flexibility on the period components. For FFT results, these periodic parts that need to be filtered in the frequency domain are set to zero. Then, the IFFT is used to regain the digital signals in the time domain (Zhao 2008).

Figure 5(c and d) are based on the filtered hemispheric SSN series. We could note the similarities and differences between the two hemispheres. Both have a period of about 64.9 months (frequency 0.0154), i.e., 5.4 years, but with different magnitudes. This also validates the cycle of about 5.3 years that we pointed out through total solar irradiance analysis in our previous study (Zhao *et al.* 2019). These demonstrate the result, i.e., solar activity that has a period about 5 years again. In addition, there is also a period 44.4 months (frequency: 0.0225) for northern hemisphere.

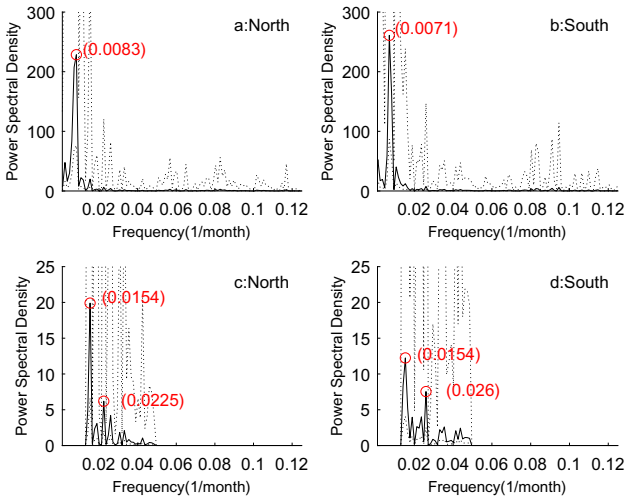

Figure 5. Power spectrum of the SSN series for the northern and southern hemispheres. (a) and (b) are the power spectra of the hemispheric SSN, respectively. (c) and (d) are based on the filtered hemispheric SSN, respectively. Dotted line indicates the 90% confidence level and red circles are periods for unfiltered and filtered SSN.

But the same scale period for southern hemisphere is about 38.5 months (frequency: 0.026). These also were revealed in Figures 3 and 4.

4. Principal component analysis and reconstruction

4.1 *Resample sunspot cycle*

As displayed in Table 1, there are 12 cycles with unequal length in the northern and southern hemispheres, respectively. The length varies from 116 to 152 months and the average is 132 months. To change the varying cycle length to the equal length for applying PCA method, we resampled the sunspot cycles to have the same length of time-steps (132 months).

4.2 *Principal component analysis*

Principal component analysis (PCA) could reduce multivariate sets to several PCs and these PCs could maintain most of the information of the original variation of solar activity, in the case of not excessive information loss, because of the dimensionality reduction technique from PCA. In general, take a smaller value m, make the accumulative contribution rate of the first m PCs not lower than a certain level to reduce dimension (Zharkova *et al.* 2012; Takalo & Mursula 2018; Zhao 2021).

The percent variance explained by:

$$\sum_{i=1}^{p} \mathrm{var}(y_i) = \sum_{i=1}^{p} \lambda_i = \sum_{i=1}^{p} \sigma_{ii} = \sum_{i=1}^{p} \mathrm{var}(x_i), \qquad (1)$$

where λ_i is the variance of the ith PC. The total variance of the original data is equal to the sum of the variances of p independent PCs.

The contribution rate of PC y_i is the variance of the ith PC y_i contributes to the total variance, $\lambda_i / \sum_{i=1}^{p} \lambda_i (i = 1, 2, \ldots, p)$. In other words, the contribution rate of the PC is the explanation power to original variables. The contribution rate of the first PC has the strongest explanation power. The sum of contribution rate of the first m ($m \leq p$) PCs, $\sum_{i=1}^{m} \lambda_i / \sum_{i=1}^{p} \lambda_i$, is called the accumulative contribution rate of the first m PCs, containing the percent variance explained by the corresponding PCs (He 2019; Chen 2020). It also indicates that how much percentages of the original variable information could be identified.

We analyzed the shape and evolution of sunspot cycles from C19 to C24 in the northern and southern hemispheres using PCA, and the results are shown in Figure 6, which shows the scores of the first, second and third PC of all cycles, respectively.

As for the northern hemisphere, the contribution rate of the first PC accounts for about 81.07%, the second PC accounts for about 7.36% and the third PC accounts for about 4.77%. The accumulative contribution rate of the first three PCs accounts for about 93.2%. As we note in Figure 6(a), the first PC ascending phase lasts for 44 months and remain high for 25 months, in the end, there is a descending phase with the length of 63 months. The second PC is the sinusoidal shape. As shown in the 13-month smoothed curve, descending phase lasts for 26 months and ascending phase lasts for 17 months. Afterward, it goes down 24 months and then, goes up to 20 months again. The third PC and its 13-month smoothed curve show that its change in magnitude is slightly smaller than that of the second PC.

As for the southern hemisphere, the contribution rate of the first PC accounts for about 78.01%, the second PC accounts for about 8.27% and the third PC accounts for about 5.77%. The accumulative contribution rate of the first three PCs accounts for about 92.05%. As shown in Figure 6(b), the first PC ascending phase lasts for 45 months, and remain high for 24 months with fluctuation at the stage, then goes down 63 months. The second PC also underwent sinusoidal shapes, but there is a phase difference

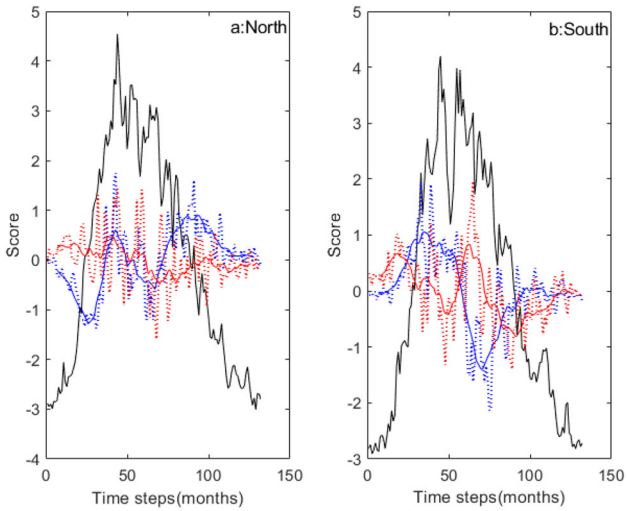

Figure 6. The scores plot of the first, second and third PC of northern and southern hemispheres, respectively. Left: For the northern hemisphere, the first PC (black solid curve), the second PC (blue dotted curve) and the third PC (red dotted curve). The 13-month smoothed second PC (blue solid curve) and the 13-month smoothed third PC (red solid curve). Right: For the southern hemisphere, the first PC (black solid curve), the second PC (blue dotted curve) and the third PC (red dotted curve). The 13-month smoothed second PC (blue solid curve) and the 13-month smoothed third PC (red solid curve).

compared with the northern hemisphere and the cycle is longer than that in the northern hemisphere. The third PC also underwent a sinusoidal shape variation and the range of change is smaller than the second PC.

4.3 *Reconstruction*

We reconstructed sunspot numbers for 12 cycles based on the first, second and third PC for the north (Figures 7 and 8) and the south (Figures 9 and 10).

Figure 7(a) is the Reconstructed Standardized SN (RSSN) of the northern hemisphere based on the first three PCs. Figure 7(b–d) is reconstructed by the first, second and third PC alone. Note that the changing characteristic of the six cycles reconstructed based on the first PC are essentially consistent and have distinctive characteristics by the second and third PC. This means that it is the second and third PC that determine the difference per cycle variation.

The reconstructed series based on the second PC (Figure 7c) vary nearly in a sinusoidal shape. However, six cycles can be classified into three groups–(C19, C20, C23), (C22, C24) and nearly

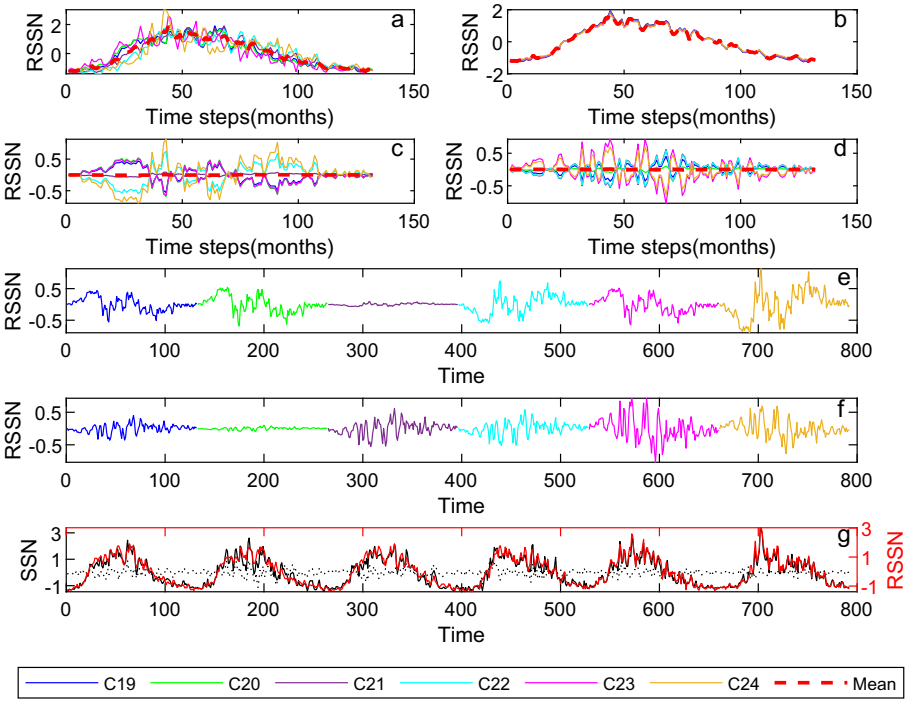

Figure 7. RSSN based on the first, second and third PC of the northern hemisphere, respectively. (a) Reconstructed based on the first three principal components. (b) Reconstructed based on the first PC. (c) Reconstructed based on the second PC. (d) Reconstructed based on the third PC. (e) The consecutive series reconstructed based on the second PC for each cycle. (f) The consecutive series reconstructed based on the third PC for each cycle. (g) Comparison between RSSN and original SSN, dotted line is the difference between the two.

unchanged C21—based on their varying characters. As (C19, C20, C23) are increased, (C22, C24) appear to show the opposite trend, a downward change and vice versa. It almost shows a changing pattern of zero-value symmetry. Furthermore, the mean cycle of the reconstructed six cycles based on the second PC, changes slightly at or near zero. We made a power spectrum analysis for two reconstructed series based on the second PC, C20 and C24, chosen from two groups with opposite trends, respectively (Figure 8a, b). We go through a reverse process that changes the equal length back to its original length because we resampled the sunspot cycles to have the same length of time-steps (132 months) earlier. Therefore, a reconstructed series whose length is equal to the original length is obtained and applied here for power spectrum analysis. The same method was adopted before the power spectrum analysis for Figures 8 and 10. We can note that series has an obvious period of about 48 months, and this is consistent with the aforementioned sinusoidal shape variation (Figure 8a, b).

Figure 7(d) is the reconstructed results based on the third PC. All cycles are classified into two groups—(C19, C23, C24) and (C20, C21, C22), and shows

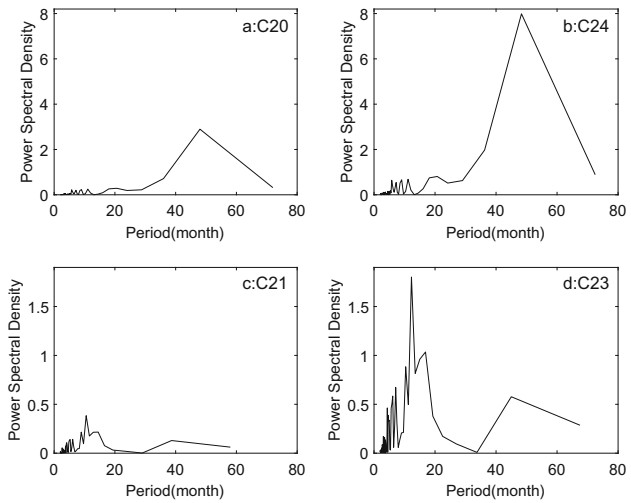

Figure 8. Power spectrum of RSSN based on the second and third PCs chosen from two groups with opposite trends, respectively, for the northern hemisphere. (a) and (b) are based on the second PC. (c) and (d) are based on the third PC.

different classification characteristics from reconstructed series based on the second PC. When (C19, C23, C24) goes up, (C20, C21, C22) goes down. Although the magnitude of the two groups is different,

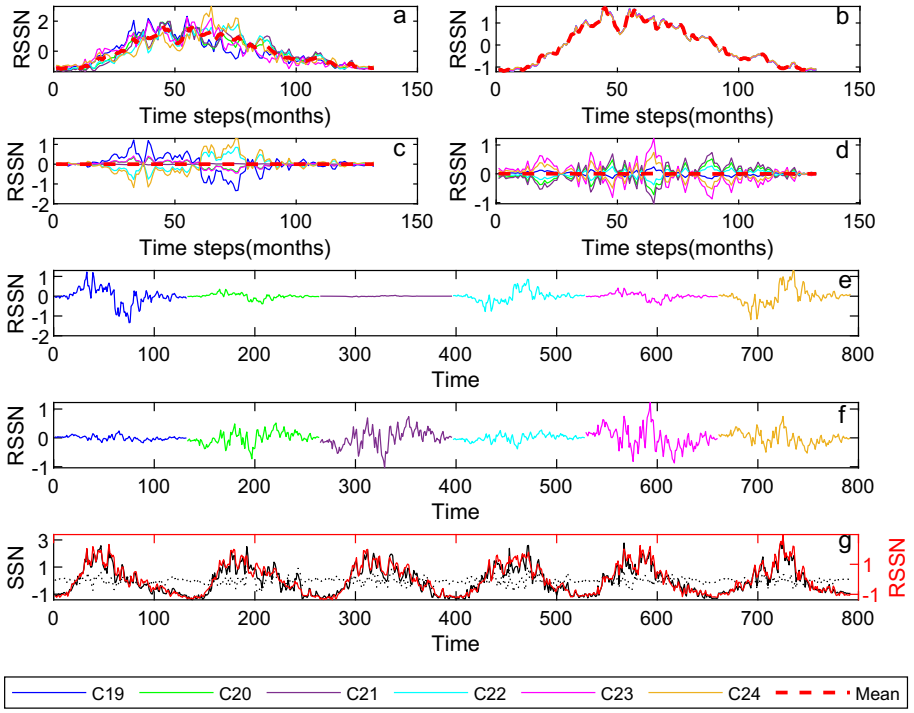

Figure 9. RSSN based on the first, second and third PC of the southern hemisphere, respectively. (a) Reconstructed based on the first three principal components. (b) Reconstructed based on the first PC. (c) Reconstructed based on the second PC. (d) Reconstructed based on the third PC. (e) The consecutive series reconstructed based on the second PC for each cycle. (f) The consecutive series reconstructed based on the third PC for each cycle. (g) Comparison between RSSN and original SSN, dotted line is the difference between the two.

the change characteristics exhibit a zero-value symmetry pattern. And the mean cycle of reconstructed six cycles also changes slightly at or near zero. Two cycles with opposite variation characteristics, C21 and C23, are also chosen for power spectrum analysis (Figure 8c, d) and have periods of about 44 and 12 months. It is better to plot them as a series to see the phase of the second and third components for each cycle in Figure 7(e and f). Some cycles based on the second PC changes with great fluctuation, but based on the third PC changes little, such as C20. However, C21 exhibits the opposite characteristics. Some cycles changes greatly, such as C24. The RSSN has been plotted along with the original SSN in Figure 7(g) and the difference between the two is shown by the dotted line. Note that the reconstruction series tallies well with the original series on the whole and most reconstructed values are consistent with the original values.

We reconstructed SSN for the southern hemisphere as north, based on the first three PCs (Figure 9a) and by the first, second and third PC alone, respectively (Figure 9b–c). As we expected, the variation characteristics of the six cycles based on the first PC are the same. However, based on second and third PCs are different, that is, similar to the northern hemisphere. From Figure 9(e and f), note the differences in the phase of the second and third components for each cycle. At the same time, compared with Figure 7(e and f), we could note the similarities and differences between the two hemispheres. For example, C21 for the south, exhibits that RSSN based on the second PC, changes little and based on the third PC, changes significantly, same as northern. However, C20 compared with north shows the opposite characteristics, that the RSSN, based on the second PC, changes little and on the third PC, changes greatly.

We can identify from the reconstructed results based on the second PC (Figure 9c) that six cycles can be classified into three groups—(C19, C20, C23), (C22, C24) and nearly unchanged C21—based on their varying character. (C19, C20, C23) and (C22, C24) present the opposite characteristics of the change. The mean cycle of the reconstructed six series based on the second PC are also at or near zero (Figure 9c), as in the northern hemisphere. Likewise, we made spectrum analysis for reconstructed series, C19 and C24, in distinct groups, based on the second PC and shown in Figure 10(a, b). Both have a period

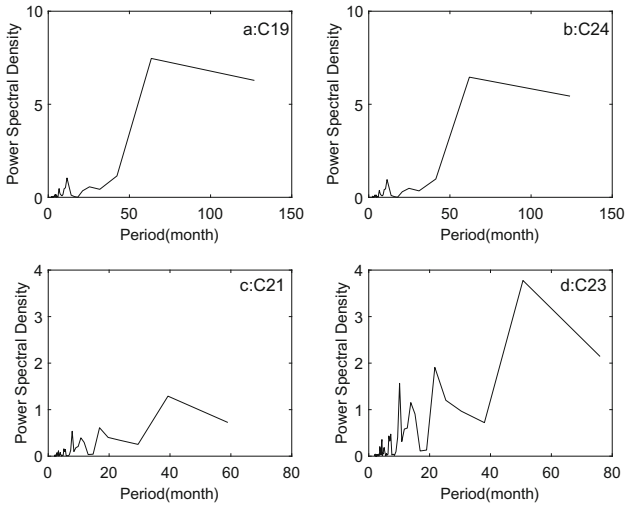

Figure 10. Power spectrum of RSSN based on the second and third PC chosen from two groups with opposite trends, respectively, for the southern hemisphere. (a) and (b) are based on the second PC. (c) and (d) are based on the third PC.

Table 2. Correlation coefficient between the reconstructed hemispheric SSN based on the first three PCs and the original SSN for cycles C19–C24.

Cycle	C19	C20	C21	C22	C23	C24
North	0.972	0.935	0.966	0.956	0.978	0.985
South	0.970	0.929	0.955	0.950	0.975	0.977

of 66 months and a period of 12 months with a smaller magnitude, respectively.

The reconstructed series based on the third PC for southern hemisphere shown in Figure 9(d) is classified into two groups, (C19, C23, C24) and (C20, C21, C22), exhibiting the opposite characteristics. Comparing power spectrum of C21 and C23 from reconstructed series based on the third PC (Figure 10c, d), there are four periods about 44, 18.9, 12 and 8.8 months in both series.

The correlation coefficients between the reconstructed hemispheric series based on the first three PCs and the original SSN for cycles C19–C24 are displayed in Table 2, respectively. The correlation coefficients are all above 99% confidence level.

The comparison of individual cycles reconstructed based on the first three PCs and based on the second PC between two hemispheres and the global sunspot are displayed in Figure 11. As shown, the shape of these cycles appears to be asymmetry not only in ascending and descending stages, but also in northern and southern cycles. The shape of global cycles (black line) and hemispheric cycles (blue and red lines) show two typical structures of sunspot cycle, single-peaked structure, such as C19, or double-peaked structure known as the Gnevyshev gap (Gnevyshev 1963), such as C24. Du (2015) speculated that the solar cycle is governed by a bi-dynamo model forming two stochastic processes depicted by a bimodal Gaussian function with a time gap of about 2 years, from which the above features can be reasonably explained.

Through the global data of the merger of two hemispheric series, we can see that C22, C23 and C24 have an obvious bimodal structure and display three different situations. One is C22. From the RSSN, based on the first three PC (Figure 11d), note that one peak is obvious and the other peak is not obvious for northern hemisphere, but the difference between the two peaks is not large. Similar trends are observable in southern hemisphere, but the main peak of south is behind the north. Therefore, global C22 cycle appears obvious double-peaked structure. Another is C24 (Figure 11f), similar to C22 (Figure 11d), but different. One is the large peak value difference between the two peaks, and the other is the long interval between the two peaks. However, the merger into the global data shows a typical bimodal structure. The third is C23 (Figure 11e), two hemispheres show a bimodal structure, respectively. It is more pronounced in the southern hemisphere than in the northern. Therefore, C23 still shows bimodal characteristics after merging into global data.

It can thus be seen that double-peaked structure occurs in two ways. In the situation A, the cycles of the southern and northern hemispheres themselves have characteristic of bimodal structure; in another situation B, the large time difference of the main peaks between two hemispheres results in the global cycle with a typical double peak, such as C24, the southern peak has reached 43 months after the northern peak.

Moreover, amplitude difference and phase difference of the RSSN, based on the second PC, have great influence on the overall RSSN, based on the first three PCs of hemispheres. For example, for C21, based on the second PC, its RSSN is less different, so there is less difference between the northern and southern hemispheres. Conversely, based on the second PC, if the RSSN changes greatly that would differentiate the shape of northern and southern hemispheres of this cycle even more, such as C24.

It is clearly shown in Figure 12 that based on the second PC, the RSSN vary along with the RSSN, based on the first three PC of C22, C23 and C24 with double peaks. The green star means the bimodal stage.

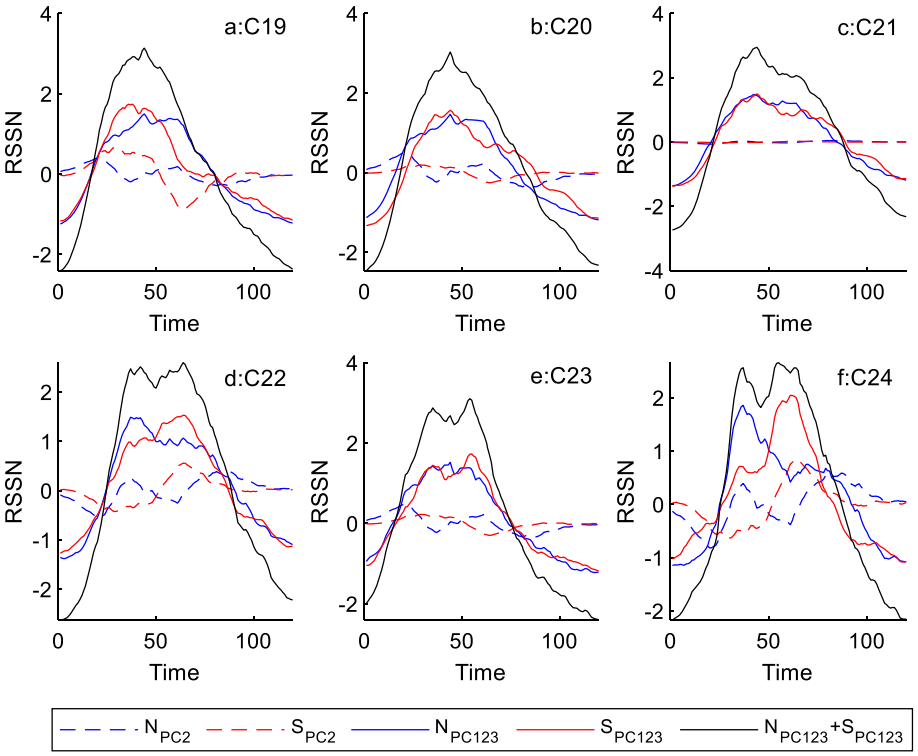

Figure 11. The comparison between northern RSSN and southern RSSN. Blue (red) solid curves shows the 13-month smoothed northern (southern) hemispheric RSSN reconstructed based on the first three principal components. Dashed line is RSSN, based on the second PC. And black line is the global RSSN from C19 to C24, respectively.

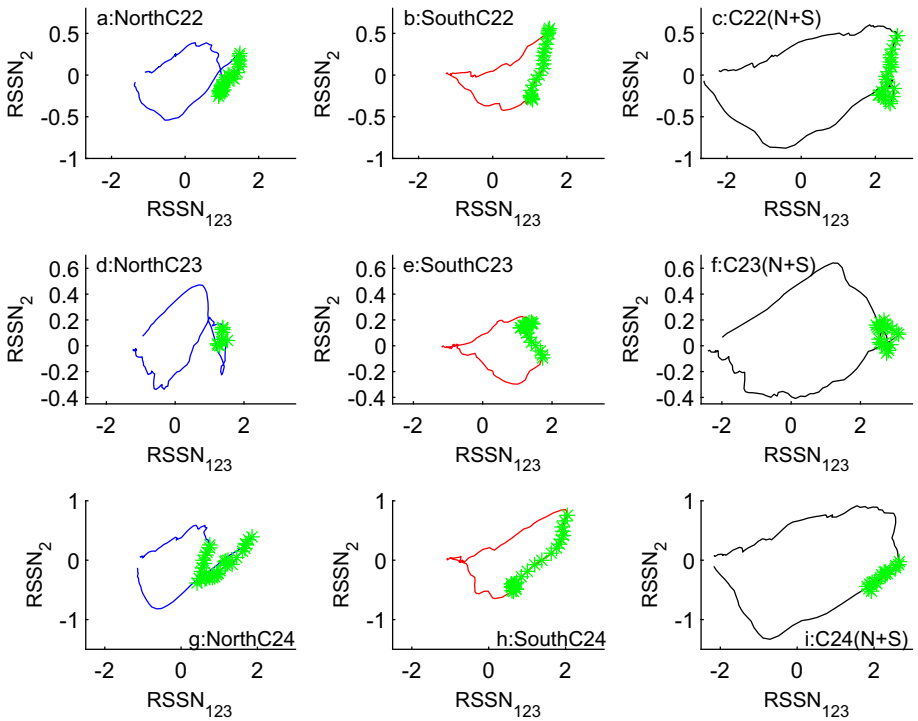

Figure 12. The RSSN reconstructed based on the first three principal components vs. the RSSN reconstructed based on the second PC for C22, C23 and C24. Blue, red and black solid curves are for northern, southern hemispheric and global (N+S) RSSN, respectively.

From Figure 12, based on the second PC, we could clearly see the value range of the northern, southern and global RSSN in the bimodal stage.

As discussed above, C23 is in situation A. In double-peaked stage, based on the second PC, the RSSN in both the northern and southern hemispheres are concentrated around the zero value. Therefore, based on the second PC, the global RSSN is concentrated around the zero. However, C22 and C24 are in situation B. Based on the second PC, although the RSSN is also around zero, the range is obviously much larger than in situation A. Based on the second PC, some even cover almost the entire range of RSSN such as southern hemisphere of C22 and C24. Therefore, the overall global effect is not as concentrated as the C23, about a third or even a half of the RSSN, based on the second PC.

5. Conclusion

The analysis presented here could contribute to understand the change patterns and characteristics the of sunspot cycle in the northern and southern hemispheres. Our main results may be summarized as follows.

Various cycles of two hemispheres, both in shape, location of the peak, length of cycle and double-peaked structure, present different characteristics. Here, cycle length varies between 116 and 152 for 12 cycles. For the same cycle, the length of the northern and southern hemispheres are not equivalent. For example, for C24, there are 21 months of difference, north 145 and south 124. However, the cumulative length of even–odd pairs approximately equal for two hemispheres.

The comparisons we have outlined, whether the results from time-varying wavelet spectral analysis or global power spectrum before and after filtering, imply the similarity and the difference in the characteristics of periods between the northern and southern hemispheres. In addition to about 11 years cycle, two hemispheres have 2–7 years short periods. For the 11-year cycle, the north is smaller than the south. Moreover, there are fundamental differences between the short periods of the two hemispheres, whether in length or strength. The magnitude characteristics of different periods in different durations are greatly inconsistent, especially in short periods.

From decomposed monthly SSN for two hemispheres of C19 to C24 using PCA, as expected, whichever hemisphere it is, the changes in characteristics of each reconstructed cycle based on the first PC, were the same. But, based on the second and third PC, they are different. Specifically, the main determinant of the variation in various cycles is the second and the third PC, whichever the hemisphere is. As for the northern hemisphere, the contribution rate of the first PC accounts for about 81.07%; and for the southern hemisphere, the contribution rate of the first PC accounts for about 78.01%. The length of ascending phase is smaller than that of descending phase, whether the north or the south, but were different for the two hemispheres. As for the northern hemisphere, the first PC ascending phase lasts 44 months. However, as for the southern hemisphere, the first PC ascending phase lasts 45 months. It means, in general, the north peaked before the south.

Based on the first, second and third PC, we reconstructed hemispheric SSN. Note that beyond the difference in the shape of RSSN, based on the first PC, between the two hemispheres, the northern and southern hemispheres show different periods features of RSSN, based on the second and third PCs. The periods of the RSSN, based on the second PC are 48 months for the north, and 66 and 12 months for the south, respectively. For the short periods of the third PC, the south is a bit more complicated than the north and has 2 periods more than the north. So in total, there are significant differences between the two hemispheres, whether the original spectrum or the spectrum of a single component. All these may turn out, therefore, the differences between the two hemispheres are quite marked.

The general characteristics of the global sunspot cycle are comprehensive results of many factors from the northern and southern hemispheres. Both hemispheres have many different characteristics. We can view not only the differences from the first PC but also the more complicated differences created by the second and third PC. All these factors were combined to create the differences in cycles between the two hemispheres, such as the double-peaked structure. Some of the global double-peaked structures could be due to existing double peaks on two hemispheres. Whereas some attribute it to the asymmetry of the two hemispheres. Because of the large time difference existing between the peaks in both hemispheres, the double peak appeared when merged to global sunspot. For example, the typical double-peaked structure of C22 is composed of two atypical bimodal structures of the northern and southern hemispheres. Therefore, the characteristic of the global sunspot cycle is the average of two hemispheres.

The difference analysis of the temporal evolution, shape of hemispheric sunspot cycles and asymmetry are of great importance to improve the understanding of the global cycle variation and its evolution, to fully understand the physical mechanism of the solar periodic variation and hemispheric asymmetry. It should be necessary to study the sun's origin, structure and evolution of the solar magnetic field, solar dynamo and so on.

Acknowledgments

This research has been supported by the National Natural Science Foundation of China (Grant No. 11203004). The data was provided by WDC-SILSO, Royal Observatory of Belgium, Brussels.

References

Chen L. 2020, Probability statistics in astronomy (Beijing: Science Press)
Du Z. L. 2015, ApJ, 804, 15
Gnevyshev M. N. 1963, SvA, 7, 311
Hale George E., Nicholson Seth B. 1925, ApJ, 270
Hathaway D. H. 2015, Living Rev. Solar Phys., 12, 4
He X. Q. 2019, Multivariate Statistical Analysis (Beijing: China Renmin University Press)
Jennings R. L., Weiss N. O. 1991, MNRAS, 252, 249
Mcclintock B. H., Norton A. A. 2013, Sol. Phys., 287, 215
Norton A. A., Charbonneau P., Passos D. 2014, Space Sci. Rev., 186, 251
Prithvi R. S. 2021, RAA, 21, 4
Schüssler M., Cameron R. H. 2018, A&A, 618, A89
Sokoloff D., Nesme Ribes E. 1994, A&A, 288, 293
Svalgaard L., Kamide Y. 2013, ApJ, 763, 23
Takalo J., Mursula K. 2018, A&A, 620, A100
Takalo J., Mursula K. 2020, A&A, 636, A11
Tobias S. M. 1997, A&A, 322, 1007
Waldmeier M. 1971, Sol. Phys., 20, 332
Waldmeir M. 1960, Zeit. Astrophys., 49, 176
Zhao J. 2008, PAAG, 165, 7
Zhao J. 2021, New Astron., 92, 1
Zhao J., Lin H. B. *et al*. 2019, JoAA, 40, 11
Zharkova V. V., Shepherd S. J., Zharkov S. I. 2012, MNRAS, 424, 2943